ECS Journal of Solid State Science and Technology, **3** (9) Q3091-Q3094 (2014)
2162-8769/2014/3(9)/Q3091/4/$31.00 © The Electrochemical Society

JSS FOCUS ISSUE ON OXIDE THIN FILM TRANSISTORS

Magnetron-Sputtered SnO Thin Films for p-Type and Ambipolar TFT Applications

H. Luo, L. Y. Liang,[z] Q. Liu, and H. T. Cao[z]

Division of Functional Materials and Nano Devices, Ningbo Institute of Material Technology and Engineering, Chinese Academy of Sciences, Ningbo 315201, People's Republic of China

SnO_x films were fabricated by reactive rf magnetron sputtering under various oxygen partial pressures (P_O = 1.6%–50%) and then annealed in an air ambient. Four operating window regions of the SnO_x films are demonstrated such as metallic Sn dominated films with n-type conduction, polycrystalline SnO dominated films with p-type conduction, SnO-SnO_2 composite films with high resistivity, and amorphous SnO_2 dominated films with n-type characteristics. TFT devices using the SnO dominated films as channels are investigated. The TFTs with the channels of a hole concentration over 10^{18} cm^{-3} show depletion p-type characteristics. The hole concentration can be tunable by changing P_O, the channel thickness, and the annealing durations. An ambipolar operating mode is obtained by modulating the hole concentration.

[DOI: 10.1149/2.017409jss]

Manuscript submitted May 30, 2014; revised manuscript received August 22, 2014. Published September 3, 2014. *This paper is part of the JSS Focus Issue on Oxide Thin Film Transistors.*

Transparent oxide semiconductors have been proposed as one of the most promising candidates used in thin film transistors (TFTs) or other complex electronic circuits on basis of their low-fabrication temperature, good transparency in visible light region, and high field-effect mobility.[1–3] However, most of high mobility oxide semiconductors show n-type conduction; only a limited number of oxides exhibit p-type conduction with modest hole mobilities. Thus, the application of oxide semiconductors is limited to unipolar n-type devices. Bipolar oxide semiconductors, in which both n-type and p-type carriers can be freely transported, are highly desirable to realize Complementary Metal–Oxide–Semiconductor (CMOS)-like devices and circuits.[4]

Generally, the valence band maxima (VBM) of oxide semiconductors is mainly composed by localized O 2*p* orbitals, which severely limits hole transport.[5] The use of hybridized orbitals between O 2*p* and metal cation n*d* (such as Ni 3*d*, Cu 3*d* and Ag 4*d*) has been proposed to make p-type oxide semiconductors.[6–8] P-type NiO and Cu_2O TFTs with a field-effect mobility of 1.6×10^{-4} cm^2/Vs and 4.3 cm^2/Vs have been demonstrated, respectively.[9,10] Similarly, tin monoxide (SnO) has been proved to be a good p-type oxide semiconductor due to the incorporation of isotropic extended Sn 5*s* orbitals into the VBM.[5,11] The p-type SnO TFTs with a field-effect mobility up to 6.75 cm^2/Vs has been reported.[12] Interestingly, SnO has a small fundamental bandgap (0.5–0.7 eV),[5,13] which favors the ambipolar behavior for electronic devices.[14] Meanwhile, it has a large direct optical bandgap (2.5–3.4 eV),[15–17] leading to rather high transparency in the visible region. In addition, it was proposed that SnO is also a good electron conductor, because the electron transport near the conduction band minimum follows a free-electron-like model.[18] Therefore, among transparent oxide semiconductors, SnO TFTs were reported to operate in an ambipolar mode.[4,18]

The SnO thin films can be prepared by several techniques, such as electron beam evaporation, pulsed laser deposition, vacuum thermal evaporation, solution process and magnetron sputtering, and so on.[4,12,18–21] Among them, the sputtering technique has the advantage of preparing large-area uniform films for large-scale industrial application.[22] Nevertheless, the previously reported SnO TFTs exhibited either p-type or ambipolar behavior.[4,18] The reason that governs the conversion from the p-type mode to the ambipolar mode was rarely reported and still not clear. In this article, SnO_x films were fabricated by reactive rf magnetron sputtering under various oxygen partial pressure (P_O). The structural evolution and electrical properties are also discussed in detail, in order to find out the operating window to fabricate SnO-dominated films. The influence of the fabrication conditions on the performance of the SnO TFTs is also discussed.

Experimental

Film fabrication and characterization.— About 200 nm-thick SnO_x films were fabricated by reactive rf magnetron sputtering applying a 2-inch Sn target (99.99%) at room temperature. The sputtering power was kept at 40 W. Ar flux (f_{Ar}) was fixed at 6 sccm, while O_2 flux (f_O) was changed ranging from 0.1 to 6 sccm. The oxygen partial pressure ($P_O = f_O/(f_{Ar} + f_O)$) was in a range of 1.6%–50%. Subsequently, the SnO_x films were annealed at 200°C in air for 1 h. The structural and electrical properties of the films were characterized by X-ray diffraction (XRD, Bruker D8 Advance X-ray diffractometer) and Hall-effect (ACCENT, HL5500) measurement, respectively.

TFT fabrication and characterization.— Top-contact and bottom-gate type TFTs were fabricated on commercial available SiO_2-Si(n^+) (SiO_2~105 nm, the gate capacitance per unit area $C_0 \sim 33$ nF/cm^2) substrates. The channel layers with a thickness of about 24 nm were sputtered with P_O as the parameter varying between 10.4% and 15.5%. Subsequently, Ni/Au source-drain electrodes were deposited by E-beam evaporation. The SnO channel layer and source-drain electrodes were patterned by shadow masks. The width and length of the TFTs were 1000 μm and 100 μm, respectively. Before depositing source-drain electrodes, SnO films were annealed in air at various temperatures (150–300°C) with different annealing durations (t_A). Output and transfer characteristics of the TFTs were measured at room temperature in the dark using a semiconductor parameter analyzer (Keithley 4200).

Results and Discussion

Thin film properties.— Fig. 1 shows the XRD patterns of the SnO_x films fabricated at various P_O. At P_O = 1.6%, both α-SnO phase (α-PbO structure, P4/nmm, JCPDS card No.06–0395) and β-Sn phase ($I4_1$/amd, JCPDS card No.19–1365) are observed in the films, but the latter one is dominated. As P_O increases, the peak intensity of the β-Sn phase decreases and becomes comparable with that of the α-SnO phase at P_O = 9.1%. At P_O = 15.5% and 16.7%, the β-Sn phase nearly disappears and only the α-SnO phase with more attenuated peak intensity is observed. When $P_O \geq 17.8\%$, no characteristic peaks are detected, suggesting the amorphous nature of the films. The phase evolution trend is consistent with our previous report.[23] It was suggested that the crystalline structure transition from polycrystalline to amorphous results from the involvement of Sn^{4+} in the SnO matrix, which boosts the structural disorder and consequently increases the crystallization temperature.[23]

Fig. 2 shows the dependency of Hall mobility and carrier concentration on different P_O. In conjunction with the crystalline phase

---

[z] E-mail: lly@nimte.ac.cn; h_cao@nimte.ac.cn

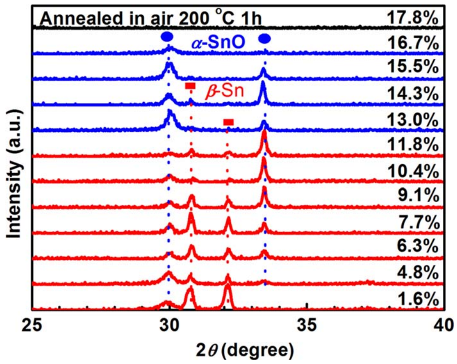

Figure 1. XRD patterns of 200 nm-thick SnO_x films deposited at different oxygen partial pressures (P_O). For clarity, only the patterns in a 2θ range of 25–40° are shown.

evolution, it can be roughly divided into four P_O regions to describe the electrical evolution of the films. (1) $P_O \leq 9.1\%$, in which the films present *n*-type conduction dominated by the metallic Sn phase. The films exhibit a very low resistivity (around $1 \times 10^{-4}\ \Omega \cdot cm$) and a high electron concentration (10^{22}–$10^{23}\ cm^{-3}$). The resistivity of the films is abnormally high at $P_O \leq 4.8\%$ because the film is discontinuous (some cracks can be observed even by the naked eyes), most probably due to the different thermal expansion coefficients between metallic Sn and SnO. (2) $9.1\% < P_O < 17.8\%$, in which the films present *p*-type conduction dominated by the polycrystalline SnO phase. In this region, the hole mobility shows an increasing trend (0.26–1.67 cm^2/Vs) and the hole concentration decreases from $10^{20}\ cm^{-3}$ to $1 \times 10^{18}\ cm^{-3}$ as P_O increases. (3) $17.8\% \leq P_O < 25\%$, where the films exhibit a rather high resistivity ($>10^4\ \Omega \cdot cm$) and pass a transition from polycrystalline to amorphous. (4) $P_O \geq 25\%$, in which the films display *n*-type behavior. In this region, the amorphous SnO_2 phase is considered to dominate other phases.[23] The conversion from p-type conduction to high resistivity and then to n-type conduction with P_O is believed to mainly originate from the competition between the donor and acceptor generation process.[23] Specifically, for the SnO-dominated films, the majority carriers are holes originated from acceptors. As the SnO_2 content increases with P_O, the acceptors are gradually compensated by the donors in the SnO_2. When the number of the acceptors has approximately the same order of magnitude as the donors, the SnO_x films would exhibit the maximum resistivity, as named as "conductivity dilemma area", which is observed for the films at P_O between 17.8% and 25%. The *n*-type behavior would be present if the donor effect is overwhelming, and vice versa.

The performance of TFTs.— Fig. 3 shows the transfer curves of TFT devices when the channel layers were deposited at $P_O = 10.4\%$–15.5%. The TFT at $P_O = 10.4\%$ displays a depletion p-type characteristic. This device cannot be turned off completely even though the gate-source voltage (V_{GS}) increases to 60 V, because the carrier concentration of the channel layer ($\sim 10^{20}\ cm^{-3}$) is too high to be depleted. As P_O increases to 11.8% or 13.0%, the TFTs show a weak ambipolar characteristic. As P_O increases to 14.3%, the drain-source current (I_{DS}) sharply decreases to $\sim 10^{-11}$ A and the device presents no TFT switching behavior, owing to the high-resistivity of the channel layer with $SnO\text{-}SnO_2$ composite phase. As P_O increases to 15.5%, the TFT displays an n-type characteristic due to the SnO_2 dominated channel.

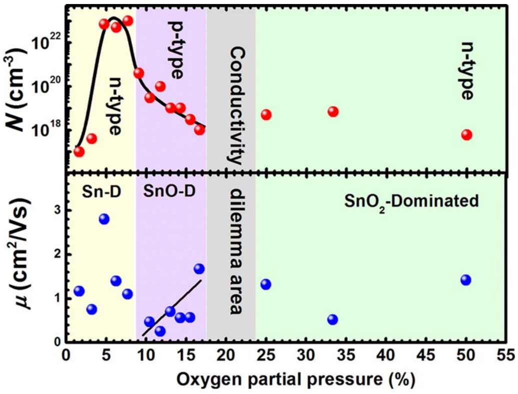

Figure 2. Hall carrier concentration *N*, and Hall carrier mobility μ vs. oxygen partial pressure (P_O) for the 200 nm-thick SnO_x films.

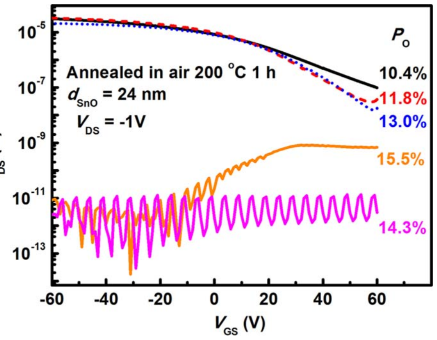

Figure 3. Transfer characteristics of TFTs with different oxygen partial pressures (P_O). d_{SnO} represents the thickness of the channel layer.

The operation mode conversion of the TFTs follows a similar variation trend with the electrical evolution of the 200 nm-thick SnO_x films (Fig. 3), but with lower P_O at which different operating modes begins to change. It is considered that a SnO_2 layer of a few nanometers is formed at the surface of the SnO_x films during the air-annealing process. With the same annealing duration, the thickness of the SnO_2 layer is almost a constant value for the SnO_x films with different thickness. Thus, the thinner SnO_x films have a higher relative content of SnO_2 which can generate a compensation for the holes, and consequently show a lower hole concentration. According to the Hall results, the hole concentration of the 24 nm-thick film ($\sim 10^{18}\ cm^{-3}$) decreases by one order compared to the 200 nm-thick one ($\sim 10^{19}\ cm^{-3}$). Also, the TFT with a 30 nm-thick channel layer shows a very low on/off current ratio (129) due to the relatively higher conductive channel, while the TFT with a 14 nm-thick channel layer demonstrates no TFT switching behavior on account of the high resistivity of the channel (as seen in Fig. 4).

It's necessary to further investigate the ambipolar TFTs. The on/off current ratio (I_{on}/I_{off}) and the linear field-effect mobility (μ_{lin}) in the *p*-channel operation are 1070 and 1.45 cm^2/Vs for the TFT at $P_O = 11.8\%$, and 1340 and 1.0 cm^2/Vs for the TFT at $P_O = 13.0\%$, respectively. The turn-on voltage (V_{on}, defined as the gate voltage at the minimum $|I_{DS}|$ in a transfer curve), reflecting the symmetry of an ambipolar TFT, is expected to be close to zero for the ambipolar TFT

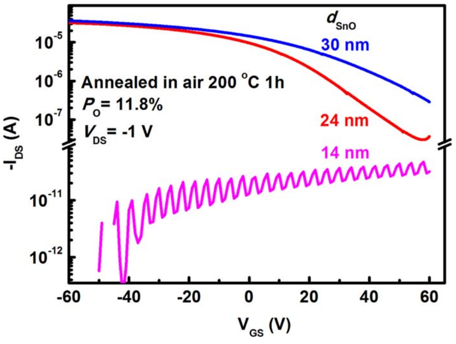

Figure 4. Transfer characteristics of TFTs with different channel thickness (d_{SnO}).

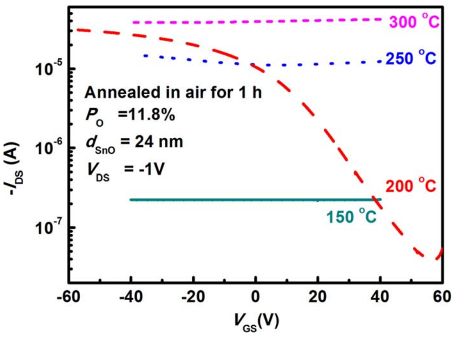

Figure 5. Transfer characteristics of TFTs annealed at different temperatures.

with good symmetry. The V_{on} is 57.8 V and 58.8 V for the TFTs at $P_O = 11.8\%$ and 13.0%, respectively. To sum up the electrical parameters, the TFT at $P_O = 11.8\%$ shows a relatively acceptable performance. Therefore, the channel layer deposited at $P_O = 11.8\%$ is selected to carry out further discussion.

Fig. 5 depicts the transfer curves of TFT devices annealed at different temperatures. The TFT annealed at 200°C shows the best performance (especially a large I_{on}/I_{off} value) as listed above. At 150°C, the I_{DS} at various V_{GS} almost keeps at -2.2×10^{-7} A, indicating that the current in the channel layer cannot be tuned by gate voltages. The most possibly reason is that the channel layer has a high resistivity and a non-ohmic contact with the source-drain electrodes. At 250°C, the device shows a weak ambipolar signal. As the annealing temperature increases to 300°C, the TFT changes into a weak n-type mode due to the SnO_2-dominated channel.

Fig. 6a displays transfer characteristics of the TFT devices annealed at 200°C in air with different durations (t_A). With increasing t_A, the on current decreases, while the off current first decreases and then rebounds when $t_A > 2$ h, which results in a maximum I_{on}/I_{off} of 1550 at $t_A = 2$ h, as shown in Fig. 6b. It should be noted that the I_{DS} at $V_{GS} > 20$ V decreases very slowly when $t_A > 4$ h, indicating that the channel layer is more and more difficult to be depleted by increasing V_{GS}. Ogo et al. had observed a similar phenomenon in SnO TFTs, and they speculated that the possible origin lies in that there are too many trap states sited at deep energies ($>\sim 0.2$ eV above the valence band) to raise the Fermi level by applying larger positive V_{GS}.[24] When $t_A > 2$ h, the deep-level trap states seem to increase as t_A, resulting in larger off currents and threshold voltages. As shown in Fig. 6b, the V_{th} decreases first and then increases with increasing annealing duration, approaching a minimum value at $t_A = 4$ h. Hall-effect measurements were also carried out, as shown in Fig. 6c. The hole concentration illustrates a decrease trend, which can couple with the decrease of the on current and the V_{th}. The Hall mobility increases with increasing t_A, opposite to the field-effect mobility evolution. As shown in Fig. 6b, the field-effect mobilities in the linear and saturation regions (μ_{lin} and μ_{sat}) monotonously decrease with t_A. In other words, long-time annealing is good for improving the hole mobility of the film, but is not desirable to improve the field-effect mobility of devices. The SiO_2 dielectric/channel interface becomes deteriorated due to a long-time annealing, leading to a more intense interface scattering. Thus, the carrier transport in the channel is greatly suppressed and consequently the field-effect hole mobility is decreased.

The TFT deposited at $P_O = 11.8\%$ and then annealed at 200°C for 2 h shows a relatively optimal performance, *i. e.*, a I_{on}/I_{off} of 1550, a μ_{lin} of 1.36 cm^2/Vs, a μ_{sat} of 0.67 cm^2/Vs in the p-channel operation, a I_{on}/I_{off} of $\sim$3 in the n-channel operation, and a V_{on} of 57 V. The output curves of the TFT are shown in Fig. 6d. In the negative V_{DS} region (the left panel), the absolute I_{DS} increases as the positive V_{GS} decreases and negative V_{GS} increases, showing a typical accumulation p-channel mode. In the positive V_{DS} region (the right panel), the I_{DS} at small V_{DS} increases as the positive V_{GS} increases, and a superlinear (diode-like) current signature presents at higher V_{DS} due to injection of the holes, showing an inversion n-channel mode.

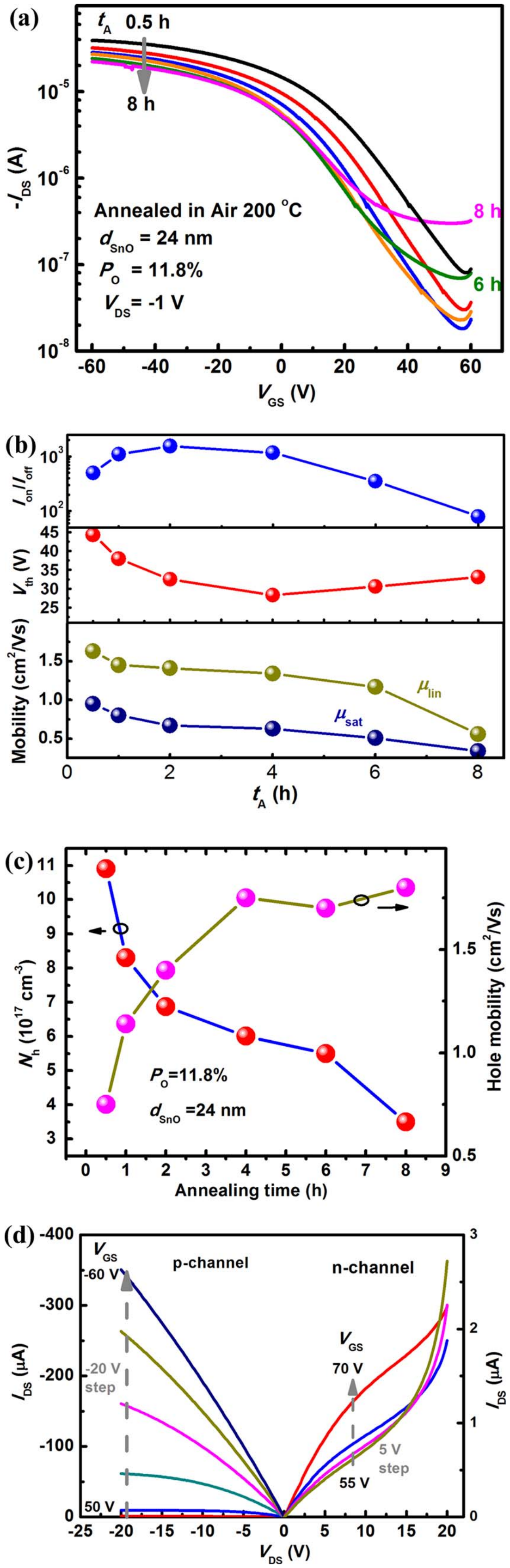

Figure 6. (a) Transfer characteristics of TFTs with different annealing durations (t_A). (b) The I_{on}/I_{off}, V_{th}, and field effect mobility ((μ_{lin} and μ_{sat}) vs. t_A, respectively. (c) Hall hole concentration and mobility vs. t_A, respectively (b) Output characteristics of the TFT deposited at $P_O = 11.8\%$ and then annealed at 200°C for 2 h.

Conclusions

SnO_x films were produced by reactive rf magnetron sputtering under various oxygen partial pressures (P_O) in conjunction with 200°C air-annealing afterwards. The structural and electrical evolution of the SnO_x films has four stages: metallic Sn dominated films with n-type conduction at Po $\leq 9.1\%$, polycrystalline SnO dominated films with p-type conduction when $9.1\% < P_O < 17.8\%$, SnO-SnO_2 composite films with high resistivity when $17.8\% \leq P_O < 25\%$, and amorphous SnO_2 dominated films with *n*-type characteristics at $P_O \geq 25\%$.

TFTs with the SnO-dominated channel are investigated. The optimal channel thickness and annealing temperature are found to be around 24 nm and 200°C, respectively. As P_O increases, the TFTs experience an interesting conversion from p-channel to plausible ambipolar working mode, mainly determined by the hole concentration. As the annealing time increases from 0.5 h to 4 h, the threshold voltage shifts to the negative position due to the decrease of the hole concentration, and the field-effect mobility slightly decreases, probably due to the enhanced interface scattering at the dielectrics/channel interface.

Acknowledgment

This work is supported by the Chinese National Program on Key Basic Research Project (2012CB933003), and the National Natural Science Foundation of China (Grant No. 11104289 and 61274095), and the Science and Technology Innovative Research Team of Ningbo Municipality (2009B21005).

References

1. J. F. Wager, *Science*, **300**, 1245 (2003).
2. K. Nomura, H. Ohta, A. Takagi, T. Kamiya, M. Hirano, and H. Hosono, *Nature*, **432**, 488 (2004).
3. Jong H. Na, M. Kitamura, and Y. Arakawa, *Appl. Phys. Lett.*, **93**, 213505 (2008).
4. k. Nomura, T. Kamiya, and H. Hosono, *Adv. Mater.*, **23**, 343 (2011).
5. Y. Ogo, H. Hiramatsu, K. Nomura, H. Yanagi, T. Kamiya, M. Hirano, and H. Hosono, *Appl. Phys. Lett.* **93**, 032113 (2008).
6. M. Taguchi, M. Matsunami, Y. Ishida, R. Eguchi, A. Chainani, Y. Takata, M. Yabashi, K. Tamasaku, Y. Nishino, T. Ishikawa, Y. Senba, H. Ohashi, and S. Shin, *Phys. Rev. Lett.*, **100**, 206401 (2008).
7. H. Kawazoe, M. Yasukawa, H. Hyodo, M. Kurita, H. Yanagi, and H. Hosono, *Nature*, **389**, 939 (1997).
8. U. K. Barik, S. Srinivasan, C. L. Nagendra, and A. Subrahmanyam, *Thin Solid Films*, **429**, 129 (2003).
9. H. Shimotani, H. Suzuki, K. Ueno, M. Kawasaki, and Y. Iwasa, *Appl. Phys. Lett.*, **92**, 242107 (2008).
10. E. Fortunato, P. Barquinha, and R. Martins, *Adv. Mater.*, **24**, 2945 (2012).
11. L. Y. Liang, Z. M. Liu, H. T. Cao, Z. Yu, Y. Y. Shi, A. H. Chen, H. Z. Zhang, Y. Q. Fang, and X. L. Sun, *J. .Electrochem. Soc.*, **157**, H598 (2010).
12. J. A. Caraveo-Frescas, P. K. Nayak, H. A. Al-Jawhari, D. B. Granato, U. Schwingenschlogl, and H. N. Alshareef, *ACS Nano*, **7**, 5160 (2013).
13. X. Q. Pan and L. Fu, *J. Electroceram.*, **7**, 35 (2001).
14. L. Y. Liang, Z. M. Liu, H. T. Cao, Y. Y. Shi, X. L. Sun, Z. Yu, A. H. Chen, H. Z. Zhang, and Y. Q. Fang, *ACS Appl. Mater. Inter.*, **2**, 1565 (2010).
15. E. J. Meijer, D. M. Leeuw, E. V. Veenendaal, S. Setayesh, B. H. Huisman, P. W. M. Blom, J. C. Hummelen, U. Scherf, and T. M. Klapwijk, *Nat. Mater.*, **2**, 678 (2003).
16. L. Y. Liang, Z. M. Liu, H. T. Cao, and X. Q. Pan, *ACS Appl. Mater. Inter.*, **2**, 1060 (2011).
17. W. Guo, L. Fu, Y. Zhang, K. Zhang, G. Graham, L. Y. Liang, Z. M. Liu, H. T. Cao, and X. Q. Pan, *Appl. Phys. Lett.*, **96**, 042113 (2010).
18. L. Y. Liang, H. T. Cao, X. B. Chen, Z. M. Liu, F. Zhuge, H. Luo, J. Li, Y. C. Lu, and W. Lu, *Appl. Phys. Lett.*, **100**, 263502 (2012).
19. H. N. Lee, H. J. Kim, and C. K. Kim, *Jpn. J. Appl. Phys*, **49**, 020202 (2010).
20. K. Okamura, B. Nasr, R. A. Brand, and H. Hahn, *J. Mater. Chem.*, **22**, 4607 (2012).
21. I. C. Chiu and I. C. Cheng, *IEEE Electron Device Lett.*, **35**, 90 (2014).
22. H. Yabuta, M. Sano, K. Abe, T. Aiba, T. Den, H. Kumomi, K. Nomura, T. Kamiya, and H. Hosono, *Appl. Phys. Lett.*, **89**, 112123 (2006).
23. H. Luo,, L. Y. Liang, H. T. Cao, Z. M. Liu, and F. Zhuge, *ACS Appl. Mater. Inter.*, **4**, 5673 (2012).
24. Y. Ogo, H. Hiramatsu, K. Nomura, H. Yanagi, T. Kamiya, M. Kimura, M. Hirano, and H. Hosono, *Phys. Status Solidi A*, **206**, 2187 (2009).